PER REVIEW

Revisiting the effect of spatial resolution on information content based on classification results

M. G. Palacio[a], S. B. Ferrero[a] and A. C. Frery[b]

[a]Universidad Nacional de Río Cuarto, Córdoba, Argentina;
[b]Universidade Federal de Alagoas, Maceió, AL,Brazil

ARTICLE HISTORY
Compiled December 6, 2018

ABSTRACT
Polarimetric Synthetic Aperture Radar (PolSAR) images are an important source of information. Speckle noise gives SAR images a granular appearance that makes interpretation and analysis hard tasks. A major issue is the assessment of information content in these kind of images, and how it is affected by usual processing techniques. Previous works have resulted in various approaches for quantifying image information content. As Narayanan, Desetty, and Reichenbach (2002) we study this problem from the classification accuracy viewpoint, focusing in the filtering and the classification stages. Thus, through classified images we verify how changing the properties of the input data affects their quality. The input is an actual PolSAR image, the control parameters are (i) the filter (Local Mean, LM, or Model Based PolSAR, MBPolSAR) and the size of their support, and (ii) the classification method (Maximum Likelihood, ML, or Support Vector Machine, SVM), and the output is the precision of the classification algorithm applied to the filtered data. To expand the conclusions, this study deals not only with Classification Accuracy, but also with Kappa and Overall Accuracy as measures of map precision. Experiments were conducted on two airborne PolSAR images. Differently from what was observed by Narayanan, Desetty, and Reichenbach (2002), almost all quality measures are good and increase with degradation, i.e. the filtering algorithms that we used always improve the classification results at least up to supports of size 7×7.

KEYWORDS
Information contents; Polarimetric SAR; Filter; Classification; MBPolSAR filter; SVM classifier.

1. Introduction

Synthetic Aperture Radar (SAR) systems have been widely employed in a single-channel configuration and have showed their ability to provide high spatial resolution data about the scene. The availability of multidimensional SAR systems has made it possible to increase the amount of available information about the surface (Medasani and Reddy 2017).

Polarimetric Synthetic Aperture Radar (PolSAR) systems emerged as an important multidimensional configuration that transmit orthogonally polarized pulses towards a target, and record the returned echo. Based on the polarization of the incident wave, the object roughness and its physical characteristics, different objects scatter the incident

CONTACT M. G.Palacio. Email: gpalacio@exa.unrc.edu.ar

waves in a manner that indicates the nature of the targets (Helmy and El-Taweel 2016). Therefore PolSAR systems provide the means for a better capture of scene information than univariate SAR (Frery, Nascimento, and Cintra 2014), allowing the characterization of the targets by means of various channels and the covariance structures among them.

The interest on PolSAR data has increased in the last years, mostly after the launch of several spaceborne missions with polarimetric capabilities. PolSAR systems provide images of the Earth in both day and night, and for almost all weather conditions. Such systems emit an electromagnetic waves with two orthogonal polarizations, horizontal and vertical, and then the receiving antenna collects the backscattered wave in both polarizations Due to the coherent interference of waves reflected from many elementary scatterers, the return is affected by speckle.

Although speckle is a true scattering measurement, the complexity of the scattering process makes it necessary to consider it noise (Foucher and López-Martínez 2014). The alterations produced by speckle can significantly degrade the perceived image quality, complicate its interpretation and analysis, and reduce the precision of target detection and classification (Ma et al. 2014). Hence, modeling and characterizing speckle, its filtering and assessing its effect on the ability to extract useful information are critical tasks (Foucher and López-Martínez 2014).

There are plenty of speckle noise reduction techniques available for one-dimensional SAR data (Argenti et al. 2013). Instead, for PolSAR data, combating speckle is still a challenging task. Any speckle filter has to suppress the noise while preserving the spatial and the polarimetric information (Torres et al. 2014).

The information content (IC) needs to be quantified before attempting to perform operations to increase it. However, it is not easily quantifiable; the same image may contain different amounts of information depending on the intended application, e.g., visualization and classification.

Narayanan, Desetty, and Reichenbach (2002) used an approach for quantifying the IC based on classification accuracy, and studied how spatial degradation affects the classification of both Landsat Thematic Mapper (TM) and Shuttle Imaging Radar-C (SIR-C) images. They modeled spatial degradation by convolving with the Local Mean (LM) filters and different sizes, and assessed the information content by the accuracy of Maximum Likelihood (ML) classification. The IC was measured as the number of correctly classified pixels in the whole image, by comparing the classified image with the ground data image.

In previous studies (Palacio, Ferrero, and Frery 2017), we followed a similar scheme, using two fully polarimetric images (an Airborne Synthetic Aperture Radar, AIRSAR, and an Uninhabited Aerial Vehicle Synthetic Aperture Radar, UAVSAR). We applied the Model-Based Polarimetric SAR (MBPolSAR) filter (López-Martínez and Fàbregas 2008) because it considers all the information provided by the covariance matrix, so it improves the estimation of the individual entries and the polarimetric information (Foucher and López-Martínez 2014). We used a Support Vector Machine (SVM) algorithm to perform the classification stage because it is well suited to handle linearly nonseparable cases (Burges 1998), which is the situation at hand. As IC measures we used Kappa, Overall Accuracy, and Classification Accuracy coefficients, derived from the Confusion Matrix obtained from testing data set. We assessed the method by visual inspection of thematic maps.

Whereas Narayanan, Desetty, and Reichenbach (2002) observed a decrease in the IC with respect to spatial degradation, our studies showed the opposite effect. To analyze if the change is mainly due to the filter or to the classifier, we propose to assess the

performance of four methods resulting from the two filters with the two classifiers. The main objectives of this article can be summarized as follows: (i) comparing the four methods resulting from the combination of filter and classification; (ii) comparing the performance of the filters (for each classifier); (iii) comparing the performance of the classifiers (for each filter); (iv) evaluating the impact of degradation in each method.

2. METHODOLOGY

To investigate if the change in our previous conclusions, compared with Narayanan, Desetty, and Reichenbach (2002), is due to the filter or to the classifier we propose to assess the performance of four methods resulting from the two filters with the two classifiers. Table 1 shows the proposed methods.

[Table 1 about here.]

2.1. *Data filtering*

For Methods 1 and 3, as in Narayanan, Desetty, and Reichenbach (2002), we first apply an adaptive Refined Lee filter (Lee, Grunes, and de Grandi 1999) of size 3×3 and use this image as input to the LM filter (Lee 1980). For Methods 2 and 4 we directly use the image as input to the MBPolSAR filter.

While speckle reduction in single-channel SAR is a relatively well-established area; cf., for instance, Argenti et al. (2013), the speckle reduction problem is more complicated for PolSAR data as speckle appears both in the intensity term of each polarization and in the phase terms (Ma, Shen, and Zhang 2016). In addition, as the PolSAR channels are usually correlated, immediate extensions of the single channel model are not available. SAR data modeling and SAR data filtering are two different aspects of the same problem, as the availability of a polarimetric noise model would make a correct signal estimation possible (López-Martínez and Fàbregas 2008).

For every resolution element, a PolSAR system measures the scattering, that can be expressed as the vector

$$\boldsymbol{s} = (S_{\mathrm{hh}}, S_{\mathrm{hv}}, S_{\mathrm{vv}})^{\mathrm{T}}, \tag{1}$$

where $(.)^{\mathrm{T}}$ indicates vector transposition, and h and v denote the horizontal and vertical polarizations, respectively. Freeman and Durden (1998) presented an important description of this three-component representation.

For point scatterers, Equation (1) characterizes completely the scattering properties of the target. Instead, for distributed scatterers, $\boldsymbol{s}$ is random and can be modeled by a multivariate zero-mean complex Gaussian distribution with parameter

$$\mathbf{C} = E\left\{\boldsymbol{s}\,\boldsymbol{s}^{*}\right\},$$

where $(.)^{*}$ is the complex conjugate transpose.

---

†the same as Narayanan, Desetty, and Reichenbach (2002).

‡the same as Palacio, Ferrero, and Frery (2017).

The covariance matrix $\mathbf{C}$ contains all the information that characterizes a distributed scatterer and must be estimated from the recorded data in Equation (1). The estimation process that is reduced to the estimation of every term of the covariance matrix, is also referred to as PolSAR speckle filtering process. The ML estimator for $\mathbf{C}$ is

$$\mathbf{Z} = \frac{1}{n}\sum_{i=1}^{n} \boldsymbol{s}_i \boldsymbol{s}_i^*, \tag{2}$$

where n is the number of looks or samples employed to estimate $\mathbf{C}$, and $\boldsymbol{s}_i, i = 1, 2, \ldots, n$, are realizations of Equation (1).

The estimated covariance matrix $\mathbf{Z}$ is a random variable that has an error with respect to the value to be recovered, $\mathbf{C}$. This error might be considered as a noise component. López-Martínez and Fàbregas (2003) have shown that under the hypothesis that $\boldsymbol{s}$ is distributed as a multivariate zero-mean complex Gaussian, speckle noise for PolSAR data is a combination of multiplicative and additive noise components:

$$\mathbf{Z} = \mathbf{C} + \mathbf{N}_{\mathrm{m}} + \mathbf{N}_{\mathrm{a}}, \tag{3}$$

where $\mathbf{N}_{\mathrm{m}}$ (with zero mean) is the multiplicative speckle noise components for all the elements of the sample covariance matrix, and $\mathbf{N}_{\mathrm{a}}$ (also with zero mean) models the additive speckle noise components which only appears in the off-diagonal elements of the sample covariance matrix. That is, the diagonal terms of the covariance matrix can be characterized by a multiplicative noise model, whereas the off-diagonal ones have the characteristics of a combined multiplicative and additive noise model (López-Martínez and Fàbregas 2008). Since $E\{\mathbf{Z}\} = \mathbf{C}$, $\mathbf{Z}$ is an unbiased estimator and therefore the multiplicative-additive model does not involve loss of polarimetric information.

López-Martínez and Fàbregas (2008) pointed out that, as one may see in Equation (2), all the elements of $\mathbf{Z}$ are obtained from two components of $\boldsymbol{s}$, thus the final model for $\mathbf{Z}$ may be derived from a generalization of a speckle noise model for the Hermitian product of two SAR images $S_p S_q^*$, where $\{p, q\} \in \{\text{hh,hv,vv}\}$.

This product can be expressed in terms of $\rho = |\rho| \exp(\mathrm{j}\phi_x)$, the complex correlation coefficient between S_p and S_q; $|\rho|$ is the coherence.

Based on the conclusions of Foucher and López-Martínez (2014), we used in previous studies (Palacio, Ferrero, and Frery 2017) the MBPolSAR filter (López-Martínez and Fàbregas 2008). This filter considers all the information provided by the covariance matrix, so it improves the estimation of the individual entries and the polarimetric information. Different processes are required to filter diagonal and off-diagonal elements of $\mathbf{Z}$. Multilook filtering is applied to the diagonal elements, while off-diagonal elements are processed differently according to the corresponding complex correlation coefficient, whose module -coherence- is estimated by ML, as in López-Martínez and Pottier (2007), in order to reduce the coherence bias.

In all methods of Table 1 we applied the filter with squared windows of sides $3, 5, 7, \ldots, 19$. In each situation, we obtained nine channels, that are used as input for the classifier.

2.2. *Classification*

The classification of images gives more information about the scene in the image than just digital values.

PolSAR classification plays an active role in many domains as a significant part of remote sensing image processing. Although many studies have reported various methods with greater classification accuracy using PolSAR data instead of conventional single polarization SAR data, the way to find an effective classifier is very important for PolSAR image classification (Aghababaee, Amini, and Tzeng 2013).

In supervised classification the user supervises the pixel classification process, by selecting representative sample sites of known cover type called Training Areas.

Narayanan, Desetty, and Reichenbach (2002) performed the supervised classification using the ML classifier (Strahler 1980). ML is a widely used method for classifying remotely sensed data (Maselli et al. 1992). It is based on the Bayes Decision Rule where a pixel is assigned to that class which has a posteriori probability greater than that for all other classes.

SVMs are a set of supervised classification methods well suited to handle linearly nonseparable cases (Burges 1998), which is the situation at hand. Among other advantages, they allow defining feature vectors with numerous and heterogeneous components (Huang et al. 2018), not requiring the specification of the probabilistic distribution of the data.

Figure 1.1 shows scatterplots of the data from the training samples in the original image shown in Figure 2, LM-filtered image (Figure 1.2), and MBPolSAR-filtered image (Figure 1.3). Only the HH (abscissas) and VV (ordinates) components are shown in log-log scale. The nonlinearity of the classification problem is clear, thus making SVM an appropriate tool for classification.

[Figure 1 about here.]

SVMs were proposed as an automatic learning system based on the statistical learning theory (Vapnik 1995). This method has captured the attention of researchers due to its successful performance in different areas such as face recognition, textual categorization, predictions, image retrieval and handwriting recognition. One of the outstanding features is its excellent generalization ability even in high dimensional spaces and with small training sets.

SVMs have been applied in a number of problems, and their use in remote sensing is spreading, leading to improved results with respect to traditional classifiers like ML (Aghababaee, Amini, and Tzeng 2013; Maulik and Chakraborty 2017). Lardeux et al. (2009) presented a brief description of a SVM concluding that it performs much better than ML under the Wishart model when applied to an optimized set of polarimetric indicators. SVMs transform feature vectors into a larger dimension space, where classes can be linearly separated. It is an optimization algorithm to determine the optimal boundary between two groups. The simplest case is the linearly separable, where there is a positive distance between groups and it is possible to choose a separation hyperplane with maximal distance to each.

Consider two classes C_1, C_2 with labels -1 and $+1$.

Given $((\boldsymbol{y}_1, r_1), (\boldsymbol{y}_2, r_2), \ldots, (\boldsymbol{y}_n, r_n))$ a training sample of size n, where $r_i = +1$ if $\boldsymbol{y}_i \in C_1$ and $r_i = -1$ otherwise, with $\boldsymbol{y}_i = (y_{i1}, y_{i2}, \ldots, y_{ip})^{\mathrm{T}} \in \mathbb{R}^p$, where p is the size of the feature space. The classification problem consists in finding an optimal hyperplane for separating the two classes, which is

$$g(\boldsymbol{y}) = \boldsymbol{w}^{\mathrm{T}}\boldsymbol{y} + w_0, \tag{4}$$

where $\boldsymbol{w}$, the support vector, is the perpendicular to the hyperplane and w_0 is a scalar. The distance from the hyperplane to the closest points of each side is called the *margin*

M. The optimal separation is the one that maximizes the distance M, which is calculated as: $M = 2\|\boldsymbol{w}\|^{-1}$. The class to which an unknown observation belongs to is determined by the application of (4): if the result is positive the observation is assigned to C_1, otherwise to C_2. Strategies have been proposed to solve classification problems with more than two classes (multiclass): one-against-all and one-against-one, here we use the latter.

However, the presence of speckle in SAR images makes classification a non-linearly separable problem; cf. Aghababaee, Amini, and Tzeng (2013); Negri et al. (2018), and Figure 1. In this case the data are mapped onto an m-dimensional ($m > p$) space through a transformation $\Phi : \mathbb{R}^p \to \mathbb{R}^m$ to go back to a linear problem. The analytical form of Φ is not required, only its scalar product $\Phi(\boldsymbol{y}_i)^{\mathrm{T}} \bullet \Phi(\boldsymbol{y})$. This product, called a *kernel* function K, is the non-linear projection of the data onto the original space (dimension p). Then, the corresponding decision function can be expressed in terms of K. There are several kernel functions; in this work we use Radial Basis Functions (RBF) with parameter $\gamma = p^{-1}$, and $p = 9$ is the dimension of our feature space. SVMs also need a penalty value for missclasification errors, usually called C; in this work we used $C = 1$.

Some authors consider a fixed parameter space and search for the configuration of (C, γ) which produces the most accurate results with respect to testing samples. For simplicity and reproducibility, we used the default values of the `libsvm` library in the `e1071` package of the `R` platform (R Core Team 2018).

For all methods of Table 1 we identified the same locations of training areas which, in turn, are different from the testing areas that are used to the classification performance stage.

2.3. *Classification with filtered image as input*

The procedure of classification used for each method of Table 1 consists of:

(1) Applying the filter (LM or MBPolSAR) with sliding windows.
(2) Selecting as features for classification the nine channels resulting from the filtering.
(3) Extracting training samples from the filtered image.
(4) Predicting all pixels of the image by the classifier (ML or SVM) and obtaining the thematic map.

The procedure is repeated for each window size.

2.4. *Validation*

To evaluate the performance of the proposed methods quantitatively we constructed a Confusion Matrix for each situation (windows of sizes $3, 5, 7, \ldots, 19$) and each method, using the same testing data set. From these matrices we calculate measures of map precision:

(a) Overall Accuracy coefficient (F), as the proportion of pixels correctly classified;
(b) Kappa coefficient (κ), as the proportion of pixels correctly classified considering all the matrix entries;
(c) Classification Accuracy coefficient (CA), as the proportion of pixels correctly classified for each class.

We also evaluate qualitatively the thematic maps by visual inspection.

The computing platform was a combination of Open Source and licensed software. The open source PolSARPro v5.1 software (Pottier and Ferro-Famil 2012) was used for the pre-processing stage. ENVI version 4.8 (Harris Geospatial Solutions 2018) was the platform of choice for extracting and validating Regions of Interest (ROIs). All the other analyses were implemented in the R version 3.5.0 (R Core Team 2018) platform.

3. EXPERIMENTAL RESULTS

We used two images: a 550×645 pixels image obtained from the AIRSAR image of San Francisco, and a 700×1100 pixels image obtained from a full polarimetric UAVSAR image of Bell Ville city, in Córdoba province, Argentina.

3.1. *San Francisco image*

AIRSAR was an airborne mission with PolSAR capabilities, designed and built by the Jet Propulsion Laboratory. Figure 2 shows a 550×645 pixels region obtained from a 900×1024 pixels full polarimetric actual image of San Francisco recorded by this sensor in the L band, acquired with four nominal looks.

We identified 5 different cover types: Grass, Sea, Urban, Vegetation and Water (areas in the Sea with water movement); their training samples are shown in Yellow, Blue, Red, Green and Cyan, respectively. Furthermore, for testing classification performance, test samples were also selected.

[Figure 2 about here.]

[Figure 3 about here.]

Figure 3 show that globally the F and κ values are similar. Filtering improves the results but the perfomances are not the same.

Applying ML classifier,

- the highest values are obtained with MBPolSAR filter (Figure 3.2);
- with LM filter the maximum value is obtained with window 9×9 (Figure 3.1);
- with MBPolSAR filter the maximum value is obtained with window 7×7 (Figure 3.2).

Applying SVM classifier,

- changing window 3×3 to 5×5 produces the most noticeable difference;
- with LM filter the maximum value is obtained with window 19×19 (Figure 3.3);
- with MBPolSAR filter the maximum value is obtained with window 11×11 (Figure 3.4).

Comparing the 4 methods,

- the worst situation is with small windows and SVM classifier, however the values increase and reach similar performance of Method 1 with window 9×9;
- the best results are obtained with MBPolSAR filter, ML classifier and windows from 5×5 to 9×9.

The most noticeable difference between SVM and ML is that the first has the best performance with greater degradation, whereas such large windows spoil the ML clas-

sification.

[Figure 4 about here.]

Figure 4 shows the analysis of classes individually. The performances are similar when the same classifier is applied. Classification accuracy takes the maximum values for Sea and Urban classes, except with 3×3 window and ML classifier; in this situation the Water is the best classified.

Numerically, Water class is well classified with ML, whereas with SVM it is the worst classified (with MBPolSAR the values are less than 75 %).

However, due to the texture of the sea, almost all the maps produced by ML wrongly allocate to Water pixels of Sea class, Figure 5. Furthermore this classifier leads to great loss of detail in the Grass class.

[Figure 5 about here.]

3.2. *Bell Ville image*

Finally, we apply the methods to the UAVSAR image of Córdoba province, Argentina, recorded in the L-band, acquired with three nominal looks. We identified four different cover types: Urban, Water, Trees and Culture; their training samples are shown in Red, Blue, Green and Orange.

Figure 6 shows the data with training samples.

[Figure 6 about here.]

[Figure 7 about here.]

Globally (Figure 7) the F and κ values are similar. Filtering improves the results, specially changing the window size from 3×3 to 5×5.

The worst situation is with Method 2 (Figure 7.2) and window 3×3, however the values increase and reach similar performance of the other methods. Almost all values are high (except for Method 2 window 3×3) and increase with degradation.

Nevertheless, with LM filter (Figures 7.1 and 7.3) the increase is most noticeable initially, up to 7×7 or 9×9 windows, and are slightly reduced for larger windows. Whereas with MBPolSAR filter (Figures 7.2 and 7.4) the performance is unstable, especially when it is classified with ML, although the variations are not very remarkable.

With windows larger than 9×9 all the methods show good and similar results.

[Figure 8 about here.]

When the classes are considered individually, Figure 8, the performances are similar when the same classifier is applied (as in San Francisco image). Classification accuracy takes the maximum values for Crops class, and the minimum for Water class (river), specially using SVM where it is the class with worst performance with all degradations.

The classes Trees and Urban are very well classified with SVM and badly classified by ML (specially with small windows).

The river is better classified by ML (although the values are just over 50 %) while with SVM and small windows the values are smaller which makes it invisible, Figure 9. In addition, the Crops area is better conserved when we use SVM.

[Figure 9 about here.]

4. CONCLUSION

As in Narayanan, Desetty, and Reichenbach (2002), we studied how the information contents are affected by spatial resolution, and we compare the performances of four methods resulting from de combination of two filters (LM and MBPolSAR) and two classifiers (ML and SVM).

Globally the F and κ values are similar.

Almost all values are good (except for San Francisco image with Method 2 and 3×3 window), and increase with degradation, i.e. filtering always improves the classification results at least up to 7×7.

For San Francisco image the most noticeable difference between SVM and ML is that the first has the best performance with greater degradations whereas these windows spoil the ML classification.

When the classes are considered individually, the performances are similar when the same classifier is applied.

Not all the classes are best classified for the same method in the same situation, as the image may contain different amounts of information depending on the application (Narayanan, Desetty, and Reichenbach 2002).

References

Aghababaee, H., J. Amini, and Y. Chang Tzeng. 2013. "Contextual PolSAR image classification using fractal dimension and support vector machines." *European Journal of Remote Sensing* 46 (1): 317–332. https://doi.org/10.5721/EuJRS20134618.

Argenti, F., A. Lapini, T. Bianchi, and L. Alparone. 2013. "A Tutorial on Speckle Reduction in Synthetic Aperture Radar Images." *IEEE Geoscience and Remote Sensing Magazine* 1 (3): 6–35.

Burges, C. 1998. "A tutorial on support vector machines for pattern recognition." *Data Mining and Knowledge Discovery* 2 (2): 121–167.

Foucher, S., and C. López-Martínez. 2014. "Analysis, Evaluation, and Comparison of Polarimetric SAR Speckle Filtering Techniques." *IEEE Transactions on Image Processing* 23 (4): 1751–1764. http://dx.doi.org/10.1109/TIP.2014.2307437.

Freeman, A., and S. L. Durden. 1998. "A three-component scattering model for polarimetric SAR data." *IEEE Transactions on Geoscience and Remote Sensing* 36 (3): 963–973.

Frery, A. C., A. D. C. Nascimento, and R. J. Cintra. 2014. "Analytic Expressions for Stochastic Distances Between Relaxed Complex Wishart Distributions." *IEEE Transactions on Geoscience and Remote Sensing* 52 (2): 1213–1226.

Harris Geospatial Solutions. 2018. *ENVI – Environment for Visualizing Images.* https://www.harrisgeospatial.com/docs/using_envi_Home.html.

Helmy, A. K., and G. S. El-Taweel. 2016. "Adaptive Local Means Filter for Polarimetric SAR Images; Despeckling for Homogeneous and Heterogeneous Clutter Models." *Information Technology and Computer Science* 11: 33–45.

Huang, Y., G. Liao, Z. Zhang, Y. Xiang, J. Li, and A. Nehorai. 2018. "SAR Automatic Target Recognition Using Joint Low-Rank and Sparse Multiview Denoising." *IEEE Geoscience and Remote Sensing Letters* in press.

Lardeux, C., P. Frison, C. Tison, J. C. Souyris, B. Stoll, B. Fruneau, and J. P. Rudant. 2009. "Support vector machine for multifrequency SAR polarimetric data classification." *IEEE Transactions on Geoscience and Remote Sensing* 47 (12): 4143–4152.

Lee, J. S. 1980. "Digital image enhancement and noise filtering by use of local statistics." *IEEE Transactions on Pattern Analysis and Machine Intelligence* 2: 165–168.

Lee, J. S., M. R. Grunes, and G. de Grandi. 1999. "Polarimetric SAR speckle filtering and

its implication for classification." *IEEE Transactions on Geoscience and Remote Sensing* 37 (5): 2363–2373.

López-Martínez, C., and X. Fàbregas. 2003. "Polarimetric SAR speckle noise model." *IEEE Transactions on Geoscience and Remote Sensing* 41 (10): 2232–2242. http://dx.doi.org/10.1109/TGRS.2003.815240.

López-Martínez, C., and X. Fàbregas. 2008. "Model-Based Polarimetric SAR Speckle Filter." *IEEE Transactions on Geoscience and Remote Sensing* 46 (11): 3894–3907.

López-Martínez, C., and E. Pottier. 2007. "Coherence estimation in synthetic aperture radar data based on speckle noise modeling." *Applied Optics* 46 (4): 544–558. http://ao.osa.org/abstract.cfmURI=ao-46-4-544.

Ma, X., H. Shen, Q. Yuan, and L. Zhang. 2014. "Spatially Adaptive Nonlocal Total Variation for PolSAR Despeckling." In *IEEE International Geoscience & Remote Sensing Symposium (IGARSS)*, Quebec City, QC, Canada, July, 1670–1676.

Ma, X., H. Shen, and L. Zhang. 2016. "PolSAR anisotropic diffusion filter with a refined similarity measure and an adaptive fidelity constraint." *International Journal of Remote Sensing* 37 (24): 5988–6011. https://doi.org/10.1080/01431161.2016.1253893.

Maselli, F., C. Conese, L. Petkov, and R. Resti. 1992. "Inclusion of prior probabilities derived from a nonparametric process into the maximum likelihood classifier." *Photogrammetric Engineering and Remote Sensing* 58: 201–207.

Maulik, U., and D. Chakraborty. 2017. "Remote Sensing Image Classification: A survey of support-vector-machine-based advanced techniques." *IEEE Geoscience and Remote Sensing Magazine* 5 (1): 33–52.

Medasani, S., and G. Umamaheswara Reddy. 2017. "Analysis and Evaluation of Speckle Filters for Polarimetric Synthetic Aperture Radar (PolSAR) Data." *International Journal of Applied Engineering Research* 12 (15): 4916–4927.

Narayanan, R. M., M. K. Desetty, and S. E. Reichenbach. 2002. "Effect of spatial resolution on information content characterization in remote sensing imagery based on classification accuracy." *International Journal of Remote Sensing* 23 (3): 537–553. http://dx.doi.org/10.1080/01431160010025970.

Negri, R. G., A. C. Frery, W. B. Silva, T. S. G. Mendes, and L. V. Dutra. 2018. "Region-Based Classification of PolSAR Data Using Radial Basis Kernel Functions With Stochastic Distances." *International Journal of Digital Earth* in press.

Palacio, M. G., S. B. Ferrero, and A. C. Frery. 2017. "Information content in SAR images: A classification accuracy viewpoint." In *2017 IEEE International Geoscience and Remote Sensing Symposium, IGARSS 2017*, Fort Worth, TX, USA, 5307–5310. https://doi.org/10.1109/IGARSS.2017.8128202.

Pottier, E., and L. Ferro-Famil. 2012. "PolSARPro V5.0: An ESA educational toolbox used for self-education in the field of POLSAR and POL-INSAR data analysis." In *2012 IEEE International Geoscience and Remote Sensing Symposium*, July, 7377–7380.

R Core Team. 2018. *R: A Language and Environment for Statistical Computing*. Vienna, Austria: R Foundation for Statistical Computing. https://www.R-project.org/.

Strahler, A. H. 1980. "The use of prior probabilities in maximum likelihood classification of remotely sensed data." *Remote Sensing of Environment* 10: 135–163.

Torres, L., S. J. S. Sant'Anna, C. da Costa Freitas, and A. C. Frery. 2014. "Speckle Reduction in Polarimetric SAR Imagery with Stochastic Distances and Nonlocal Means." *Pattern Recogn.* 47 (1): 141–157. https://doi.org/10.1016/j.patcog.2013.04.001.

Vapnik, V. N. 1995. *The nature of statistical learning theory*. New York, NY, USA: Springer-Verlag New York, Inc.

List of Figures

Figures

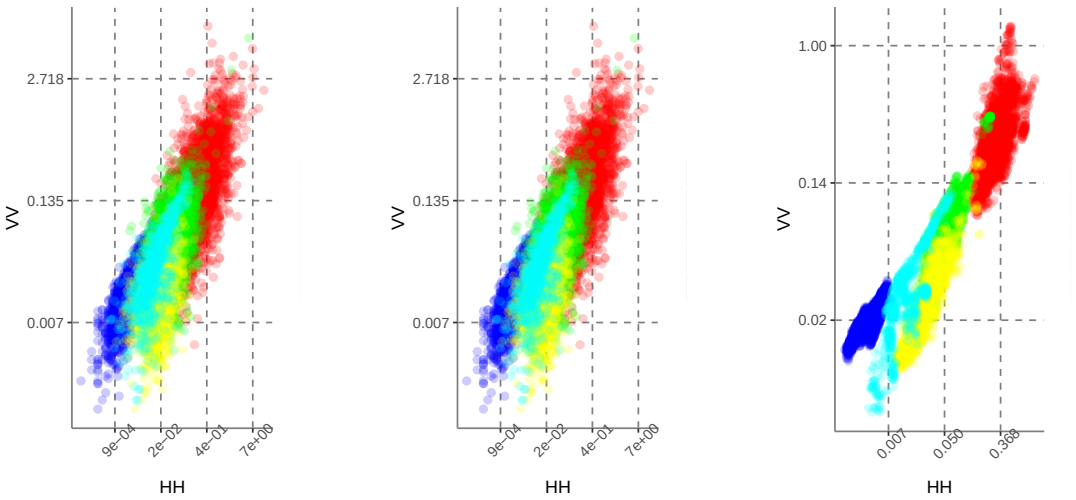

1.1: Original image

1.2: LM-filtered image

1.3: MBPolSAR-filtered image

Figure 1.: Observations from the training samples by Class

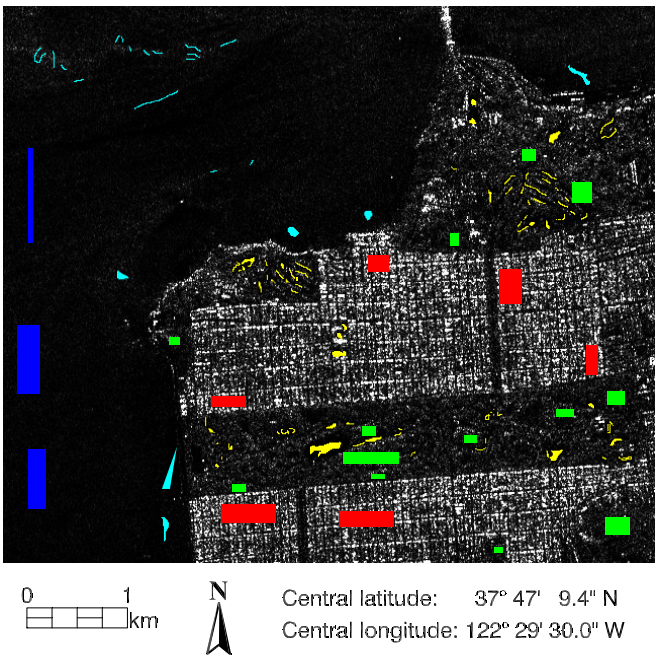

Figure 2.: AIRSAR HH data and training samples.

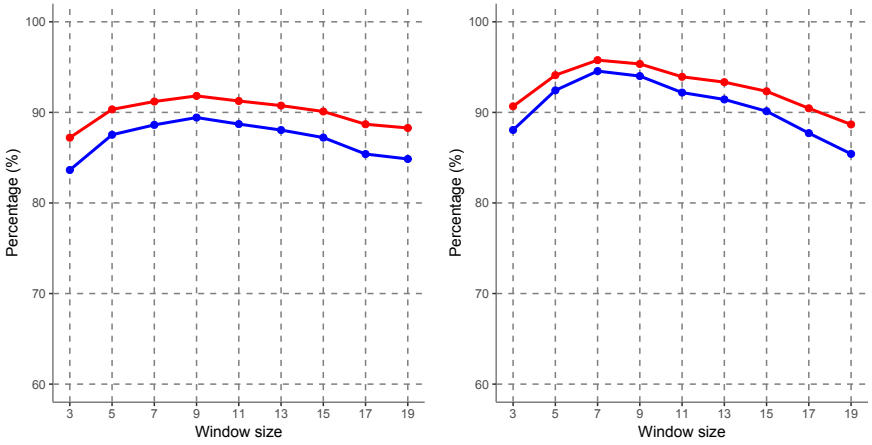

3.1: Method 1

3.2: Method 2

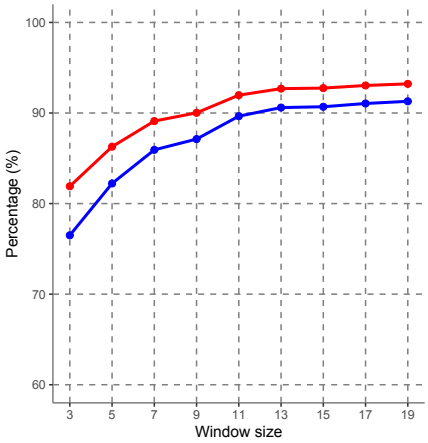

3.3: Method 3

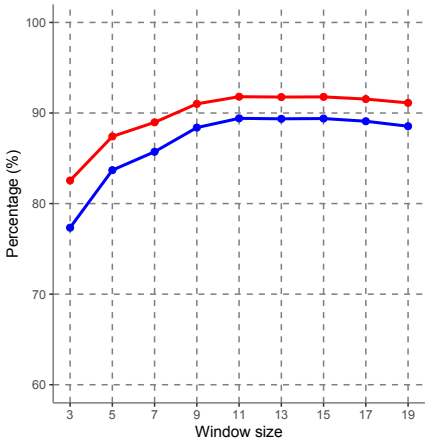

3.4: Method 4

Figure 3.: AIRSAR data. Classification performance, with coefficients F (red) and κ (blue), by window size.

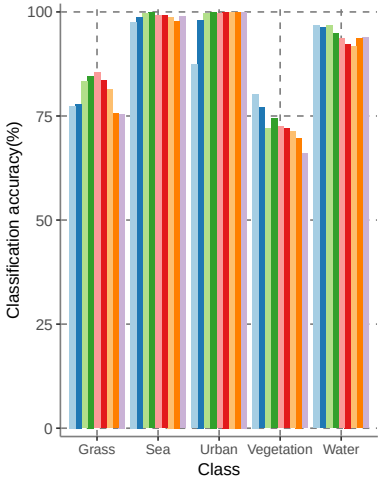

4.1: Method 1

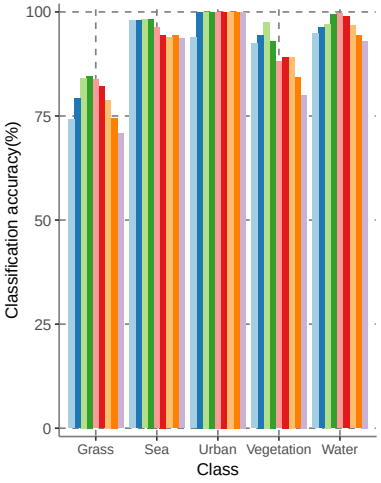

4.2: Method 2

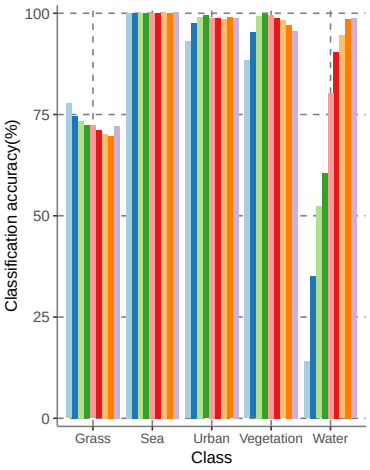

4.3: Method 3

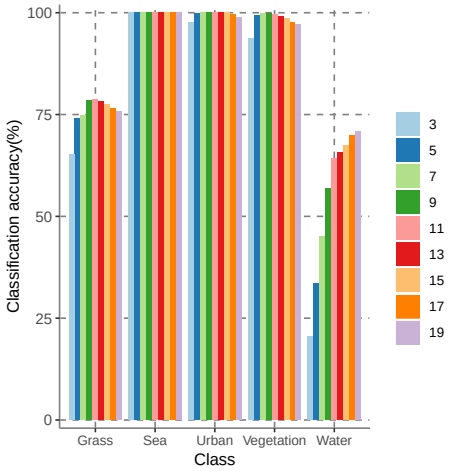

4.4: Method 4

Figure 4.: AIRSAR data. Classification performanceby class, for different windows size.

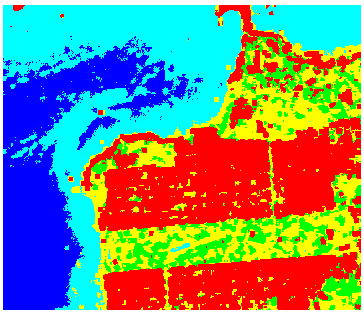

5.1: Method 1

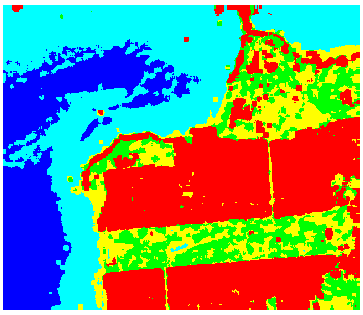

5.2: Method 2

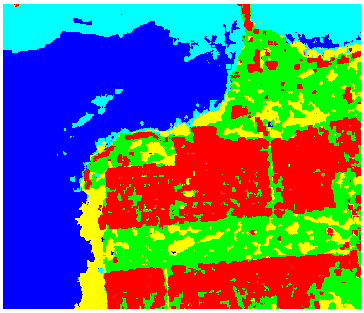

5.3: Method 3

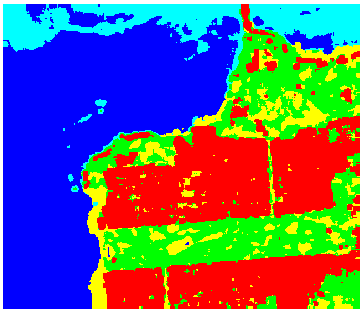

5.4: Method 4

Figure 5.: AIRSAR data. Thematic maps using 9×9 windows.

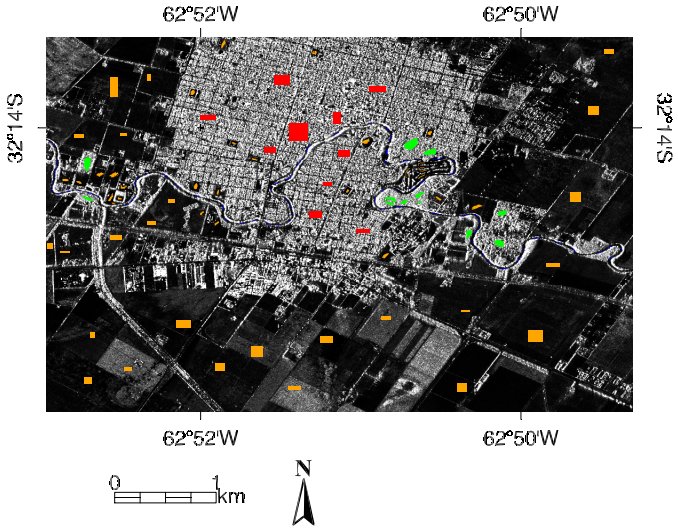

Figure 6.: UAVSAR data and training samples.

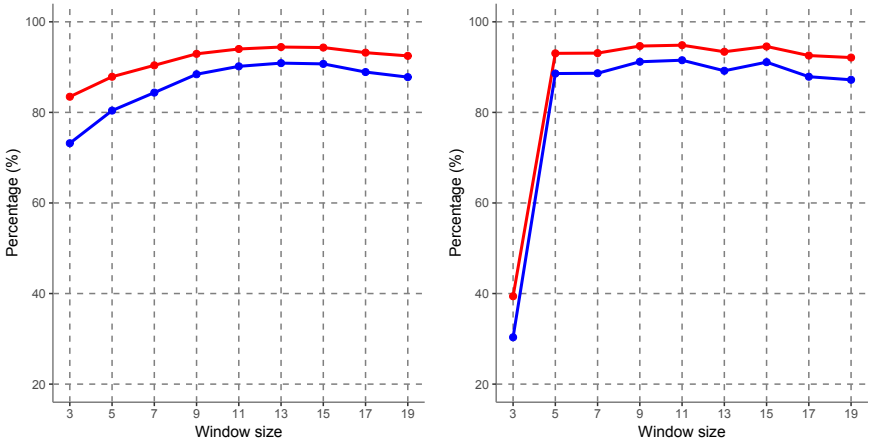

7.1: Method 1

7.2: Method 2

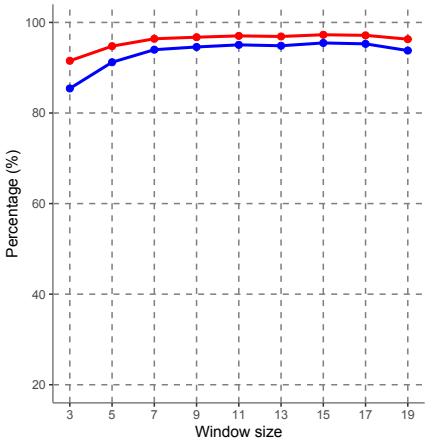

7.3: Method 3

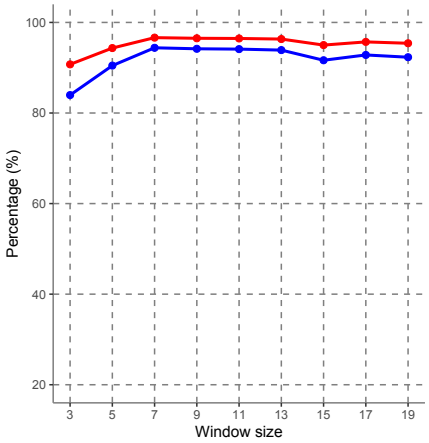

7.4: Method 4

Figure 7.: UAVSAR data. Classification performance, with coefficients F (red) and κ (blue), by window size.

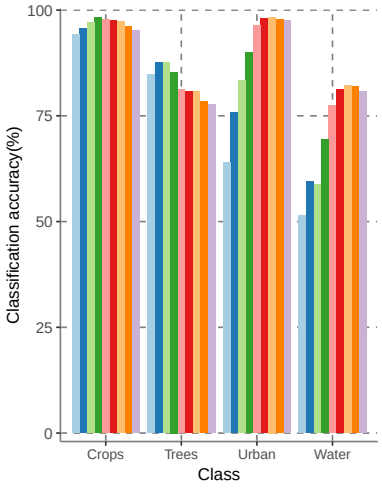

8.1: Method 1

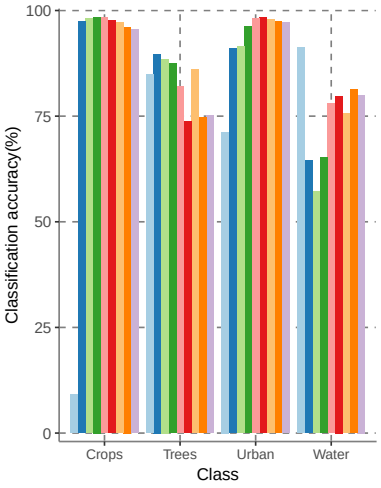

8.2: Method 2

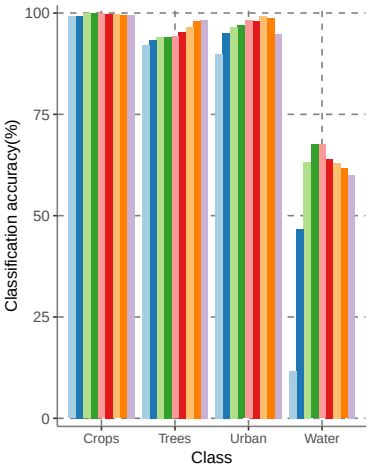

8.3: Method 3

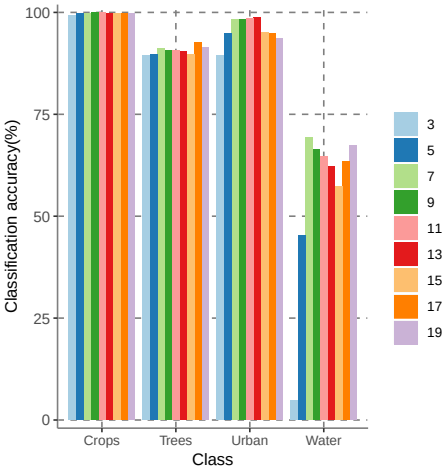

8.4: Method 4

Figure 8.: UAVSAR data. Classification performance by class, for different windows size.

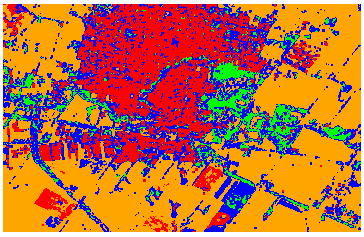

9.1: Method 1

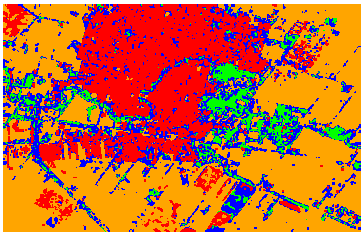

9.2: Method 2

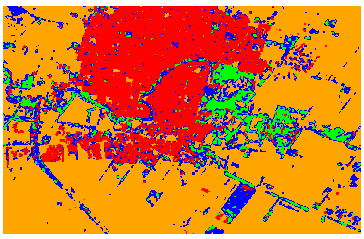

9.3: Method 3

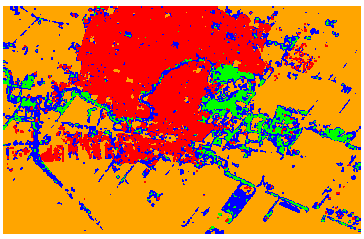

9.4: Method 4

Figure 9.: UAVSAR data. Thematic maps using 7×7 window.

List of Tables

Tables

Table 1.: Methods to compare.

	Filter	
Classifier	Local Mean	Model Based PolSAR
Maximum Likelihood	Method 1†	Method 2
Support Vector Machine	Method 3	Method 4‡